Full Title: High affinity Na^+ transport by wheat HKT1;5 is blocked by K^+

Running title: HKT1;5 proteins catalyse dual affinity Na^+ transporter in wheat

Authors: Bo Xu[1,2], Maria Hrmova[2] and Matthew Gilliham[1,2*]

[1]Australian Research Council Centre of Excellence in Plant Energy Biology, University of Adelaide, Waite Research Precinct, Glen Osmond, South Australia 5064, Australia

[2]School of Agriculture, Food and Wine, and Waite Research Institute, University of Adelaide, Waite Research Precinct, Glen Osmond, South Australia 5064, Australia

[*]Corresponding author: e-mail: matthew.gilliham@adelaide.edu.au

Abstract

The wheat sodium transporters TmHKT1;5-A and TaHKT1;5-D are encoded by genes underlying major shoot Na^+ exclusion loci *Nax2* and *Kna1* from *Triticum monococcum* (Tm) and *Triticum aestivum* (Ta), respectively. In contrast to HKT2 transporters that have been shown to exhibit high affinity K^+-dependent Na^+ transport, HKT1 proteins have, with one exception, only been shown to catalyse low affinity Na^+ transport and no K^+ transport. Here, using heterologous expression in *Xenopus laevis* oocytes we show that both TmHKT1;5-A and TaHKT1;5-D encode dual (high and low) affinity Na^+-transporters with the high-affinity component being abolished when external K^+ is in excess of external Na^+. The low-affinity component for Na^+ transport of TmHKT1;5-A had a lower K_m than that of TaHKT1;5-D even when blocked by external K^+. We use 3-D structural modelling to explain how K^+ block may occur and propose potential physiological consequences of K^+ block. The transport properties and localisation of wheat HKT1;5 proteins are well suited for their role in a 'gatekeeper' process that secure shoot Na^+-exclusion and underpin recent advances for improving crop plant salt tolerance.

Keywords: salinity; High-affinity K Transporters; HKT; wheat; membrane transport; crop; 3-D structural modelling

Introduction

Crops suffer reduced growth and productivity under salinity stress. Salt, when it builds up to high concentrations in the growing medium (i.e. soil solution) imposes an osmotic limitation on water uptake, interferes with optimal nutrient homeostasis, and leads to the build up of leaf cellular sodium (Na^+) concentrations, which causes an ionic toxicity that limits photosynthesis and carbon assimilation in plants (Munns and Gilliham, 2015).

A major genetic mechanism contributing towards salinity tolerance of most crops including the cereals rice (*Oryza sativa*) and wheat (*Triticum aestivum* and *Triticum monococcum*) is Na^+ exclusion from leaves, with the High-affinity potassium (K^+) transporter (HKT) protein family having a major role in this trait (Ren *et al.* 2005; James *et al.* 2006; Munns *et al.* 2012; Munns and Gilliham, 2015; Campbell *et al.* 2017; Xu *et al.* 2018). This family of proteins are represented widely across the plant kingdom, and more broadly are members of the high affinity K^+/Na^+ transporting Ktr/TrK/HKT superfamily of proteins that are present in bacteria (Ktr and TrK), fungi (TrK) and plants (HKT) (Sentenac and Bonneaud 1992; Corratgé-Faillie *et al.* 2010).

These plant HKTs are divided into 2 clades: 1) class 1 HKT proteins (HKT1;x) are mostly Na^+-selective transporters; 2) whereas class 2 HKTs (HKT2;y) mostly function as K^+-Na^+ symporters and so far have been only identified in cereal monocots (Asins *et al.* 2013; Waters *et al.* 2013). This definition has been challenged on occasion, such as for OsHKT2;4 following its characterization in *Xenopus laevis* oocytes, where there are conflicting reports on its permeability to Ca^{2+}, Mg^{2+} and NH_4^+ in addition to K^+ and Na^+ (Lan *et al.* 2010; Horie *et al.* 2011; Sassi *et al.* 2012). Furthermore, there are two reports of K^+ permeability in the HKT1 clade . Firstly, Arabidopsis AtHKT1 could complement K^+ transport deficient *E. coli* although no K^+ permeability could be found when it was expressed in *X. laevis* oocytes in the same study (Uozumi *et al.*, 2000). Secondly, *Eucalyptus camaldulensis* EcHKT1;1 and EcHKT1;2, which appear to be the exception for the HKT1 proteins characterized so far in that as they transport both Na^+ and K^+ when expressed in *X. laevis* oocytes (Liu *et al.* 2001). Other HKT1 transporters have no reported K^+ permeability (Uozumi *et al.* 2000; Mäser *et al.* 2002; Platten *et al.* 2006; Jabnoune *et al.* 2009; Cotsaftis *et al.* 2012; Munns *et al.* 2012; Waters *et al.* 2013; Byrt *et al.* 2014; Campbell *et al.* 2017; Henderson et al., 2018).

Whilst K^+ transport is not a common feature of HKT1 transporters, several have shown the property of K^+-regulated Na^+ transport (Ben Amar *et al.* 2013; Almeida *et al.* 2014a; Almeida *et al.* 2014b; Byrt *et al.* 2014). For instance, the presence of 10 mM external K^+ ($[K^+]_{ext}$) reduced the inward Na^+ current of *X. laevis* oocytes expressing *HKT1;5* from *T. aestivum* (*TaHKT1;5-D*) at -140 mV (Byrt *et al.* 2014), and the outward Na^+ current of that expressing *HKT1;2* from *Solanum lycopersicum* (*SlHKT1;2*) (Almeida *et al.* 2014a). Interestingly, $[K^+]_{ext}$ stimulated both inward and outward Na^+ transport of *X. laevis* oocytes expressing two *HKT1;4* alleles from *Triticum turgidum* L. subsp. *durum* when assayed with solutions of very low ionic strength (Ben Amar *et al.* 2013).

Ktr/TrK/HKT proteins are predicted to consist of 8 transmembrane domains that fold into 4 pseudo-tetramers around a central pore (Mäser *et al.*, 2002; Cotsaftis *et al.*, 2012; Xu *et al.*, 2018). The selectivity filter lining the pore of Ktr and TrK and class 2 HKT proteins is predicted to be composed of four glycine residues. In class 1 HKTs the first glycine within the predicted selectivity filter is substituted with a serine (Mäser *et al.*, 2002); the lack of K^+ permeability in this clade has been linked to the presence of this glycine (Uozumi *et al.*, 2000; Mäser *et al.*, 2002; Platten *et al.*, 2006; Cotsaftis *et al.*, 2012; Waters *et al.*, 2013); but the exact mechanism underlying this block is to be determined.

Here, we further characterise HKT1;5 proteins underlying two major salt tolerance associated loci, *TmHKT1;5-A* (*Nax2*) and *TaHKT1;5-D* (*Kna1)* from *T. monococcum and T. aestivum* respectively. We find that both TmHKT1;5-A and TaHKT1;5-D encode dual affinity Na^+-transporters and that their dual affinity Na^+ transport can be blocked by raising external K^+ concentration, and we propose the residues within the selectivity filter that cause this block. This is the first report that Na^+ transport has two affinities in the HKT1 clade and demonstrates that dual affinity transport is a common property of both clades of the HKT family.

Results

K^+ sensitivity of TmHTK1;5-A and TaHKT1;5-D

Previously, it was shown that inward Na^+ transport for both TmHKT1;5-A and TaHKT1;5-D was inhibited by external K^+ (Munns *et al.* 2012; Byrt *et al.* 2014). Here, we further compared the K^+-sensitivity of between TmHKT1;5-A and TaHKT1;5-D (Fig. 1). An increase in $[K^+]_{ext}$ to 30 mM reduced the channel conductance of TmHKT1;5-A at -140 mV by approximately 75% in a 1 mM Na^+ ($[Na^+]_{ext}$) bath solution; similarly this amount of K^+ inhibited that of TaHKT1;5-D up to 95 % (Fig. 1A, B and Fig. 2). However, such Na^+-inhibition by K^+ was gradually decreased by increasing $[Na^+]_{ext}$ (Fig 1 and 2). For instance, 10 mM $[K^+]_{ext}$ suppressed the channel conductance of TmHKT1;5-A by 43.5% in 1 mM $[Na^+]_{ext}$ and by 16.5% in 10 mM $[Na^+]_{ext}$; it similarly reduced the TaHKT1;5-D conductance by 57% in 1 mM $[Na^+]_{ext}$ and by 23% in 10 mM $[Na^+]_{ext}$ (Fig. 1 and 2). When $[Na^+]_{ext}$ was increased to 30 mM, the channel conductance of TmHKT1;5-A was insensitive to $[K^+]_{ext}$, whereas that of TaHKT1;5-D was still inhibited (Fig. 2).

The increase in $[K^+]_{ext}$ from 0 to 10 mM did not significantly change the reversal potential of TmHKT1;5-A or TaHKT1;5-D; all reversal potentials were close to the theoretical equilibrium potential for Na^+ under all conditions (Fig. 3A,B). Moreover, the observed shift in reversal potential was close to the theoretical Nernst shift for Na^+ regardless of the presence or absence of 10 mM $[K^+]_{ext}$ (Fig. 3). This suggests that neither of protein were permeable to K^+.

Dual affinity transport of Na^+ by TmHTK1;5-A and TaHKT1;5-D

The affinity for Na^+ transport of TmHKT1;5-A was previously reported to be ~4-fold higher than the Na^+-transport affinity of TaHKT1;5-D (Munns *et al.* 2012; Byrt *et al.* 2014; Xu *et al.* 2018), which we confirm here (Fig. 4A,B). On closer examination, we found a property that has not been described before. When lower concentrations of $[Na^+]_{ext}$ were present it was clear that the concentration dependence of inward Na^+ currents could be fitted by two components, for both TmHKT1;5-A and TaHKT1;5-D (Fig. 4). Whilst both components were saturable, the concentration at which both phases saturated were greater for TaHKT1;5-D compared to TmHKT1;5-A (Fig. 4A,B). For TmHKT1;5-A, the high affinity component of Na^+ transport had a K_m of 34 µM ± 26 µM when $[Na^+]_{ext}$ was below 0.1 mM ($K_{m\ (< 0.1\ Na)}$), whereas at

concentrations of Na^+ above 0.1 mM the K_m was 1.04 ± 0.17 mM ($K_{m\ (> 0.1\ Na)}$) (Fig. 4A). The K_m for the higher affinity component of inward Na^+ transport for TaHKT1;5-D was 29 µM ± 4 µM when $[Na^+]_{ext}$ was lower than 0.5 mM ($K_{m\ (< 0.5\ Na)}$), whilst the lower affinity phase had a K_m of 4.32 ± 0.5 mM when $[Na^+]_{ext}$ was higher than 0.5 mM ($K_{m\ (> 0.5\ Na)}$) (Fig. 4B).

We examined the extent of K^+-inhibition of both the lower and higher affinity components of the inward Na^+ currents when $[K^+]_{ext}$ was 10 mM. The (normalised) inward Na^+ current catalysed by both proteins was significantly suppressed by 10 mM $[K^+]_{ext}$, resulting in negligible inward Na^+ transport by TmHKT1;5-A in presence of $[Na^+]_{ext}$ below 0.1 mM, or by TaHKT1;5-D in presence of $[Na^+]_{ext}$ below 0.5 mM (Fig. 4C and D). In the presence of 10 mM $[K^+]_{ext}$ it was now possible to fit the concentration dependence of inward current through TmHKT1;5-A and TaHKT1;5-D with one component. The K_m of both TmHKT1;5-A and TaHKT1;5-D were decreased approximately by 3-fold by 10 mM $[K^+]_{ext}$ (Fig. 4E and F).

Structural modelling of TaHKT1;5-D

Three-dimensional structural models of TaHKT1;5-D were generated to explore why K^+ does not traverse the pore but instead blocks the Na^+ currents, using the KtrB K^+ transporter from *B. subtilis* as a template (Vieira-Pires *et al.*, 2013; Xu *et al.*, 2018). The KtrB K^+ protein was crystallised in the presence of KCl, hence the original structure contained a K^+ ion in the selectivity filter region. This ion was substituted by Na^+ during modelling of TaHKT1;5-D as it transports Na^+ but not K^+ (Xu *et el.*, 2018). Ramachandran analysis indicated that the template and TaHKT1;5-D models generated in complex with Na^+, and K^+ had satisfactory stereo-chemical quality; Ramachandran plots showed only two residues positioned in disallowed regions (0.5% of all residues, except G and P residues). Average G-factors (measures of correctness of dihedral angles and main-chain covalent forces of protein molecules) calculated by PROCHECK of the template and TaHKT1;5-D models with K^+ and Na^+ were 0.06. -0.18 and -0.13, respectively. The ProSa 2003 analysis of z-scores (-8.4; -6.0 and -5.8) indicated that template and modelled structures with K^+ and Na^+ had acceptable conformational energies.

The TaHKT1;5-D model showed that the Na^+ ion is penta-hedrally coordinated with

V76, S77, S78, N231, C232 and H351 (all carbonyl oxygens), that lie near the selectivity filter residues S78, G233, G353 and G457 (Fig. 5A). Notably, the carbonyl oxygen one of the selectivity filter residues (S78) directly participates in Na^+ binding (Fig. 5A). Conversely, the K^+ ion is hexa-hedrally coordinated with V76, N231, C232, H351, N455 and V456, that also closely neighbour the selectivity filter residues (Fig. 5B); here none of the selectivity filter residues participate in direct binding of K^+. The ionic distances of residues neighbouring Na^+ and K^+ ions are within similar ranges: for Na^+ they are between 2.3 and 2.4 Å; for K^+ they are between 2.6 and 2.9 Å (Fig. 5, right panels).

Discussion

Oocytes expressing *TmHKT1;5-A* or *TaHKT1;5-D* have been previous reported to undergo no obvious change in their reversal potential regardless of the presence or absence of K^+ in bath solution. Interestingly, both transporters had differential sensitivity to external $[K^+]_{ext}$. Whilst K^+ block occurs for TmHKT1;5-A catalysing inward transport it was not evident at $[Na^+]_{ext}$ above 10 mM, whereas this blockage did happen for TaHKT1;5-D up to 30 mM $[Na^+]_{ext}$ (Fig. 2) (Munns *et al.* 2012; Byrt *et al.* 2014). This differential inhibition effect of K^+ upon Na^+ transport at high $[Na^+]_{ext}$ by TaHKT1;5-D may result from a range of factors, that govern the rates of Na^+ and K^+ ion binding and subsequent Na^+ transport. A variety of factors could control the transport of Na^+ and preliminary displacement of competing K^+ with a consequent energetic cost, before Na^+ passes bare or less-well hydrated than competing K^+. Examples include free-energy variations between ions in binding sites relative to the corresponding quantity in bulk water, differences in selectivity filters solvent exposures (or dielectric constants), overall pore rigidity/stiffness (Dudev and Lim 2010), structural changes within funnels and selectivity filters due to residue re-orientation, differences in the hydration (coordination) numbers of Na^+ and K^+ (Na^+ and K^+ bind six and seven water molecules, respectively (Rowley and Roux 2012) and the alterations on the rates of Na^+ or K^+ de-solvation (Degrève *et al.* 1996). It is therefore plausible to expect that both ions would compete for binding sites within HKT funnel regions, yielding ion-protein binding sites with differential binding strengths.

Here, we refine the previous structural models of HKT1;5 to show that they contain a pore that allows the passage of Na^+ but not K^+ (Cotsaftis *et al.*, 2012; Waters *et al.*, 2013; Xu *et al.*, 2018). This is consistent with the functional observations in this and previous studies (Munns *et al.* 2012; Byrt *et al.* 2014). Previously it was suggested that the Gly-Gly-Gly-Gly motif is important in coordinating the K^+ ion in Ktr/TrK transporters and in conferring dual Na^+-K^+ transport in HKT2 transporters (Durrell and Guy, 1999; Mäser *et al.* 2002). Here our modelling suggests that the serine residue within the Ser-Gly-Gly-Gly selectivity motif directly interacts and binds with Na^+ (Fig 5B). Furthermore, our model suggests, despite ionic distances being shorter for Na^+ than those for K^+, that K^+ could be bound more strongly due to a higher coordination pattern (Fig. 5A and 5B-right panels). Obviously, during binding, K^+ takes an advantage of its larger ionic radius: 152 picometer (pm), compared to that of Na^+ (116 pm); these parameters reflects empirical atomic radii of K (220 pm) and Na (180 pm). We assume that under the high concentrations of K^+, this ion may outcompete Na^+ and would become bound in the selectivity filter, thus effectively blocking Na^+ transport. This is illustrated by calculating permeation channels in both complexes, using the Mole Voronoi algorithm, that predicts permeation trajectories and identifies path bottlenecks. From the calculated permeation paths, it could be deduced that the K^+ ion effectively blocks the permeation channel through the major gating protein pore, contrary to Na^+. It is also obvious that Na^+ is likely to enter and exit the permeation trajectory from several points on both sides of the transporter, but always by-passes the selectivity filter constriction. Both ions arrive at the funnel of HKT proteins in solvated (hydrated) forms. While the hydration number for Na^+ is 6, that for K^+ is 7 at ambient temperature (Rowley and Roux 2012; Ma, 2016). The significance of the seven-fold water coordination for K^+ is that this solvated complex may form a stronger hydrogen-bond interaction pattern (in funnels of HKT proteins), and would be de-solvated with a higher energy input and thus slower) that the Na^+ solvated complex (Degrève et al., 1996). It is also plausible to expect that both solvated ion complexes would compete for binding sites within HKT funnel regions with different binding strengths. All in all, this would contribute to the blockage of the pore entry of HKT transporters.

Potassium permeability for HKT1 transporters has only been reported once for the proteins that have been characterised in *X. laevis* oocytes. The transporters EcHKT1;1

and EcHKT1;2 allow permeation of both K^+ and Na^+ (Liu *et al.*, 2001). Interestingly, when 3D models of the Na^+ selective OsHKT1;5 and K^+ permeable EcHKT1;2 were constructed and compared the pore size was predicted to be 0.2 Å larger in EcHKT1;2 (than OsHKT1;5 and TaHKT1;5-D), which would more than account for the weaker interactions with K^+ and allow this larger ion to pass through the pore (Waters *et al.*, 2013). Without 3D modelling of each and every transporter in the HKT family to show how the selectivity filter forms in the context of the rest of the protein it would not be possible to predict which other HKT1s may allow passage of K^+. Predictions based on sequence alone are insufficient to predict how the two sets of proteins evolved their individual Na^+ and K^+ transport characteristics. An extension of the model to include other HKT proteins, a greater survey of structure-function relationships and mutations of key residues to predict functionally relevant residues and evolutionary relationships will be the focus of further study.

Two affinity ranges for Na^+ transport have been detected in the HKT family previously, but only for HKT2 transporters. OsHKT2;1, OsHKT2;2, OsHKT2;4 and HvHKT2;1(Schachtman and Schroeder 1994; Rubio *et al.* 1995; Jabnoune *et al.* 2009; Yao *et al.* 2010; Horie *et al.* 2011; Sassi *et al.* 2012). For instance, for OsHKT2;2, when K^+ is present, the transport of Na^+ is K^+-dependent and displays a high affinity (K_m = 0.077 mM), whereas showing a lower affinity when absence of K^+ (K_m= 16 mM) (Rubio *et al.* 1995; Yao *et al.* 2010). OsHKT2;1 also acquires two phases of Na^+-transport affinity, whose K_m for Na^+ is respectively 9.5 µM at $[Na^+]_{ext}$ below 1 mM and is 2.2 mM at $[Na^+]_{ext}$ > 1 mM (Jabnoune *et al.* 2009). The K^+ transport catalysed by HvHKT2;1 is affected by both $[Na^+]_{ext}$ and $[K^+]_{ext}$, such as a decrease in its K^+ transport affinity from 30 µM down to 3.5 mM by $[Na^+]_{ext}$ increased from 0.5 mM to 30 mM and a greatly reduced channel conductivity for K^+ by increasing $[K^+]_{ext}$ above ~3 mM (Mian *et al.* 2011). This is the first time that dual affinity characteristics have been reported for the HKT1;*x* family (Fig. 4). Considering the considerably homology between both clades (58% similarity/41% identity between TaHKT1;5 and TaHKT2;1) it is perhaps not surprising that both clades can confer dual affinity transport. How such ability is conferred structurally is still to be determined.

In summary, whilst the high-affinity component was similarly inhibited by 10 mM $[K^+]_{ext}$ for both TaHKT1;5-D and TmHKT1;5-A, the low affinity component of Na^+

transport for TmHKT1;5-A was less inhibited by external K than TaHKT1;5-D (Fig. 4). Furthermore, both wheat HKT1;5 proteins facilitate Na^+ uptake at high affinity; TmHKT1;5-A facilitates Na^+ uptake with a higher affinity than TaHKT1;5-D regardless the absence or presence of $[K^+]_{ext,}$ (Fig. 4) (Munns *et al.* 2012; Byrt *et al.* 2014). TmHKT1;5-A has been shown to be more effective in conferring shoot Na^+ exclusion to wheat compared to TaHKT1;5-D (James *et al.*, 2012). We propose that the higher affinity (with half-maximal activity nearer 1 mM compared to 4 mM), and a lower sensitivity to $[K^+]_{ext}$ are both characteristics that can help confer better shoot Na^+ exclusion, which is a property that can lead to greater salt tolerance in the field for wheat (James *et al.* 2011; James *et al.* 2012; Munns *et al.* 2012).

Materials and Methods

Brief methods for cloning of *TmHKT1;5-A* and *TaHKT1;5-D* as well as its functional characterisation in heterologous expression systems were described Munns et al. (Munns *et al.* 2012) and Byrt et al. (Byrt *et al.* 2014). Further details are included here.

Two-electrode voltage clamp recording in *X. laevis* oocytes

Oocyte recording followed the methods as described in Munns et al. (Munns *et al.* 2012)and Byrt et al. (Byrt *et al.* 2014). Briefly, 46 nl/23 ng of cRNA or equal volumes of RNA-free water were injected into oocytes, followed by an incubation for 48 h before recording. Membrane currents were recorded in the HMg solution (6 mM $MgCl_2$, 1.8 mM $CaCl_2$, 10 mM MES and pH 6.5 adjusted with a TRIS base) ± Na^+ glutamate and/or K^+ glutamate as indicated. All solution osmolarities were adjusted using mannitol at 220-240 mOsmol kg^{-1}.

Construction of 3D models of TaHKT1;5D in complex with Na^+ and K^+ ions

The most suitable template for TaHKT1;5D, the KtrB K^+ transporter from *B. subtilis* (Protein Data Bank accession 4J7C, chain I) (Vieira-Pires et al., 2013), was identified as previously described (Xu et al., 2017). The KtrB K^+ protein was crystallised in the presence of KCl, hence the structure contains a K^+ ion in the selectivity filter region. This ion was substituted by Na^+ during modelling of TaHKT1;5D that transport Na^+ at a greater rate than K^+ (Xu et el., 2017). 3D structural models in complex with Na^+, and K^+ were generated using Modeller 9v16 (Sali and Blundell, 1993) on a Linux station

running the Fedora 12 operating system, as previously described (Cotsaftis et al., 2012, Waters et al., 2013, Xu et al., 2017). During modelling, attention was paid to ionic radii of Na^+, and K^+, whose topology parameters were taken from CHARMM (Brooks et al., 2009). In each case, a total of 100 models were generated that were scored by Modeller using the modeller objective function (Shen and Sali, 2006), the discrete optimised protein energy function (Eswar et al., 2008), PROCHECK (Laskowski et al., 1993), ProSa 2003 (Sippl, 1993) and FoldX (Schymkowitz et al., 2005). Best scoring models constructed in Modeller 9v19 were further subjected to energy minimisation (knowledge-based Yasara2 forcefield with parameters for bond distances, planarity of peptide bonds, bond angles, Coulomb terms, dihedral angles, and van der Waals forces) (Krieger et al., 2004) combined with the particle-mesh-Ewald (PME) energy function for long range electrostatics (cutoff 8.0 Å), to obtain smoothed electrostatic potentials. Structural images were generated with PyMOL Molecular Graphics System V1.8.2.0 (Schrődinger LLC, Portland, OR, USA).

Funding

This work was supported by funding to M.G. from the Grains Research and Development Corporation (UA00145, M.G.), and Australian Research Council through the Centre of Excellence (CE1400008) and Future Fellowship (FT130100709) schemes.

References

Almeida, P, de Boer, G-J, de Boer, AH (2014a) Differences in shoot Na^+ accumulation between two tomato species are due to differences in ion affinity of HKT1;2. *Journal of Plant Physiology* **171**, 438-447.

Almeida, P, Feron, R, de Boer, G-J, de Boer, AH (2014b) Role of Na^+, K^+, Cl^-, proline and sucrose concentrations in determining salinity tolerance and their correlation with the expression of multiple genes in tomato. *AoB Plants* **6**, plu039.

Asins, MJ, Villalta, I, Aly, MM, Olias, R, Álvarez De Morales, P, Huertas, R, Li, J, JAIME-PÉREZ, N, Haro, R, Raga, V (2013) Two closely linked tomato HKT coding genes are positional candidates for the major tomato QTL involved in Na^+/K^+ homeostasis. *Plant, Cell & Environment* **36**, 1171-1191.

Ben Amar, S, Brini, F, Sentenac, H, Masmoudi, K, Véry, A-A (2013) Functional characterization in Xenopus oocytes of Na^+ transport systems from durum wheat reveals diversity among two HKT1; 4 transporters. *Journal of experimental botany* **65**, 213-222.

Byrt, CS, Xu, B, Krishnan, M, Lightfoot, DJ, Athman, A, Jacobs, AK, Watson-Haigh, NS, Plett, D, Munns, R, Tester, M (2014) The Na^+ transporter, TaHKT1;5-D, limits shoot Na^+ accumulation in bread wheat. *Plant Journal* **80**, 516-526.

Campbell, MT, Bandillo, N, Al Shiblawi, FRA, Sharma, S, Liu, K, Du, Q, Schmitz, AJ, Zhang, C, Véry, A-A, Lorenz, AJ (2017) Allelic variants of OsHKT1; 1 underlie the divergence between indica and japonica subspecies of rice (*Oryza sativa*) for root sodium content. *PLoS genetics* **13**, e1006823.

Corratgé-Faillie, C, Jabnoune, M, Zimmermann, S, Véry, A-A, Fizames, C, Sentenac, H (2010) Potassium and sodium transport in non-animal cells: the Trk/Ktr/HKT transporter family. *Cellular and Molecular Life Sciences* **67**, 2511-2532.

Cotsaftis, O, Plett, D, Shirley, N, Tester, M, Hrmova, M (2012) A two-staged model of Na^+ exclusion in rice explained by 3D modeling of HKT transporters and alternative splicing. *PLoS One* **7**, e39865.

Degrève, L, Vechi, SM, Junior, CQ (1996) The hydration structure of the Na^+ and K^+ ions and the selectivity of their ionic channels. *Biochimica et Biophysica Acta (BBA)-Bioenergetics* **1274**, 149-156.

Dudev, T, Lim, C (2010) Factors governing the Na^+ vs K^+ selectivity in sodium ion channels. *Journal of the American Chemical Society* **132**, 2321-2332.

Henderson SW, Dunlevy JD, Wu Y, Blackmore DH, Walker RR, Edwards EJ, Gilliham M, Walker AR (2018) Functional differences in transport properties of natural HKT1;1 variants influence shoot Na^+ exclusion in grapevine rootstocks. *New Phytologist* **217**, 113-1127.

Horie, T, Brodsky, DE, Costa, A, Kaneko, T, Schiavo, FL, Katsuhara, M, Schroeder, JI (2011) K^+ transport by the OsHKT2; 4 transporter from rice with atypical Na^+ transport properties and competition in permeation of K^+ over Mg^{2+} and Ca^{2+} ions. *Plant Physiology* **156**, 1493-1507.

Jabnoune, M, Espeout, S, Mieulet, D, Fizames, C, Verdeil, J-L, Conéjéro, G, Rodríguez-Navarro, A, Sentenac, H, Guiderdoni, E, Abdelly, C (2009) Diversity in expression patterns and functional properties in the rice HKT transporter family. *Plant Physiology* **150**, 1955-1971.

James, RA, Blake, C, Byrt, CS, Munns, R (2011) Major genes for Na^+ exclusion, *Nax1* and *Nax2* (wheat *HKT1; 4* and *HKT1; 5*), decrease Na+ accumulation in

bread wheat leaves under saline and waterlogged conditions. *Journal of experimental botany* **62**, 2939-2947.

James, RA, Blake, C, Zwart, AB, Hare, RA, Rathjen, AJ, Munns, R (2012) Impact of ancestral wheat sodium exclusion genes *Nax1* and *Nax2* on grain yield of durum wheat on saline soils. *Functional Plant Biology* **39**, 609-618.

James, RA, Davenport, RJ, Munns, R (2006) Physiological characterization of two genes for Na^+ exclusion in durum wheat, *Nax1* and *Nax2*. *Plant Physiology* **142**, 1537-1547.

Lan, W-Z, Wang, W, Wang, S-M, Li, L-G, Buchanan, BB, Lin, H-X, Gao, J-P, Luan, S (2010) A rice high-affinity potassium transporter (HKT) conceals a calcium-permeable cation channel. *Proceedings of the National Academy of Sciences, U.S.A.* **107**, 7089-7094.

Liu, W, Fairbairn, DJ, Reid, RJ, Schachtman, DP (2001) Characterization of two HKT1 homologues from *Eucalyptus camaldulensis* that display intrinsic osmosensing capability. *Plant Physiol.* **127**, 283-294.

Mäser, P, Hosoo, Y, Goshima, S, Horie, T, Eckelman, B, Yamada, K, Yoshida, K, Bakker, EP, Shinmyo, A, Oiki, S (2002) Glycine residues in potassium channel-like selectivity filters determine potassium selectivity in four-loop-per-subunit HKT transporters from plants. *Proceedings of the National Academy of Sciences, U.S.A.* **99**, 6428-6433.

Mian, A, Oomen, RJ, Isayenkov, S, Sentenac, H, Maathuis, FJ, Véry, AA (2011) Over-expression of an Na^+-and K^+-permeable HKT transporter in barley improves salt tolerance. *Plant Journal* **68**, 468-479.

Munns, R, James, RA, Xu, B, Athman, A, Conn, SJ, Jordans, C, Byrt, CS, Hare, RA, Tyerman, SD, Tester, M, Plett, D, Gilliham, M (2012) Wheat grain yield on saline soils is improved by an ancestral Na^+ transporter gene. *Nature Biotechnology* **30**, 360-364.

Munns, R, Gilliham, M (2015) Salinity tolerance of crops - What is the cost? *New Phytologist* **208**, 668-673.

Platten, JD, Cotsaftis, O, Berthomieu, P, Bohnert, H, Davenport, RJ, Fairbairn, DJ, Horie, T, Leigh, RA, Lin, H-X, Luan, S (2006) Nomenclature for HKT transporters, key determinants of plant salinity tolerance. *Trends in Plant Sciences* **11**, 372-374.

Ren, Z-H, Gao, J-P, Li, L-G, Cai, X-L, Huang, W, Chao, D-Y, Zhu, M-Z, Wang, Z-Y, Luan, S, Lin, H-X (2005) A rice quantitative trait locus for salt tolerance encodes a sodium transporter. *Nature Genetics* **37**, 1141-1146.

Rowley, CN, Roux, Bt (2012) The solvation structure of Na^+ and K^+ in liquid water determined from high level ab initio molecular dynamics simulations. *Journal of chemical theory and computation* **8**, 3526-3535.

Rubio, F, Gassmann, W, Schroeder, JI (1995) Sodium-driven potassium uptake by the plant potassium transporter HKT1 and mutations conferring salt tolerance. *Science* **270**, 1660.

Sassi, A, Mieulet, D, Khan, I, Moreau, B, Gaillard, I, Sentenac, H, Véry, A-A (2012) The rice monovalent cation transporter OsHKT2; 4: revisited ionic selectivity. *Plant Physiology* **160**, 498-510.

Schachtman, DP, Schroeder, JI (1994) Structure and transport mechanism of a high-affinity potassium uptake transporter from higher plants. *Nature* **370**, 655-658.

Sentenac, H, Bonneaud, N (1992) Cloning and expression in yeast of a plant potassium ion transport system. *Science* **256**, 663.

429 Uozumi, N, Kim, EJ, Rubio, F, Yamaguchi, T, Muto, S, Tsuboi, A, Bakker, EP,
430 Nakamura, T, Schroeder, JI (2000) The Arabidopsis HKT1 gene homolog
431 mediates inward Na^+ currents in *Xenopus laevis* oocytes and Na^+ uptake in
432 *Saccharomyces cerevisiae*. *Plant Physiology* **122**, 1249-1260.
433 Waters, S, Gilliham, M, Hrmova, M (2013) Plant high-affinity potassium (HKT)
434 transporters involved in salinity tolerance: structural insights to probe
435 differences in ion selectivity. *International Journal of Molecular Sciences* **14**,
436 7660-7680.
437 Xu, B, Waters, S, Byrt, CS, Plett, D, Tyerman, SD, Tester, M, Munns, R, Hrmova, M,
438 Gilliham, M (2018) Structural variations in wheat HKT1; 5 underpin
439 differences in Na^+ transport capacity. *Cellular and Molecular Life Sciences* 1-
440 12.
441 Yao, X, Horie, T, Xue, S, Leung, H-Y, Katsuhara, M, Brodsky, DE, Wu, Y,
442 Schroeder, JI (2010) Differential sodium and potassium transport selectivities
443 of the rice OsHKT2; 1 and OsHKT2; 2 transporters in plant cells. *Plant*
444 *Physiology* **152**, 341-355.
445
446

Figures

Figure 1. K^+-sensitivity of Na^+ currents carried by TmHKT1;5-A and TaHKT1;5-D. A-D, current-voltage (I/V) curves of Na^+ currents recorded from *X. laevis* oocytes expressing *TmHKT1*;5-*A* (A, C) and *TaHKT1*;5-*D* (B, D) in 1 mM Na^+ plus 0-30 mM K^+ (A,B), or 0-30 mM Na^+ solutions with or without 10 mM K^+ (C,D). Mean ± S.E.M, n = 5-6.

Figure 2. Channel conductance of TmHKT1;5-A and TaHKT1;5-D. The channel conductance of TmHKT1;5-A and TaHKT1;5-D was calculated from Figure 1, based on the slope of curve between -140 mV and -120 mV, statistical difference was determined by *Students' t-test*, $*P < 0.05$ and $** P < 0.01$.

Figure 3. Shift in reversal potential of TmHKT1;5-A and TaHKT1;5-D in response to changes in $[Na^+]_{ext}$ and $[K^+]_{ext}$.
A, Reversal potential of currents in *X. laevis* oocytes expressing *TmHKT1*;5-*A* and *TaHKT1*;5-*D* derived from Figure. 1. B, Reversal potential of Na^+ currents plotted against theoretical Nernst potential derived from internal concentrations measured in Munns et al. (2012) and Byrt et al., (2014) at the used.
Nernst shift in oocytes expressing *TmHKT1*;5-*A* and *TaHKT1*;5-*D* from 1 mM to 10 mM Na^+ ($[1\text{-}10]_{ext}$ Na^+) and 10 mM to 30 mM Na^+ ($[10\text{-}30]_{ext}$ Na^+) with or without 10 mM $[K^+]_{ext}$, $\Delta Exp._{Na}$ = experimentally measured shift in reversal potential for Na^+, the theortectical equilibrium (or Nernst) potential for Na^+ was 57.7 mV and 26.9 mV, respectively for $[1\text{-}10]_{ext}$ Na^+ and $[10\text{-}30]_{ext}$ Na^+, refers to Munns et al. (2012).

Figure 4. Transport affinity of TmHKT1;5-A and TaHKT1;5-D in *X. laevis* oocytes.
A-B, dual Na^+-transport affinity of TmHKT1;5-A and TaHKT1;5-D in *X. laevis* oocytes, plotted as normalised currents at -140 mV as shown against a series of Na^+ glutamate solutions. C-D, high affinity phase of TmHKT1;5-A and TaHKT1;5-D in absence and presence of 10 mM $[K^+]_{ext}$. Data represented in A, B and C as mean ± S.E.M (n = 5 for A, n = 4 for B, n = 7 for C). E-F, Na^+-transport affinity of TmHKT1;5-A and TaHKT1;5-D in *X. laevis* oocytes, plotted as normalised currents at -140 mV as shown against a series of Na^+ glutamate solutions with an additional 10 mM K^+ glutamate.

Figure 5. Molecular models of TaHKT1;5D in complex with Na^+ (A) and K^+ (B) ions.

(A-B; left panels) Cartoon representations of TaHKT1;5-D illustrate their overall protein folds with cylindrical α-helices, and permeation channels (black mesh). Na^+ (A) and K^+ (B) ions are shown as purple spheres located within the selectivity filter residues S78, G233, G353 and G457 (coloured in cpk magenta), and other neighbouring residues. Na^+ is likely to enter and exit the permeation trajectory from several points on both sides of the transporter, but always by-passes the selectivity filter constriction. K^+ enters the selectivity filter and effectively blocks the gating trajectory.

(A-B; right panels) Detailed views of bound Na^+ and K^+ ions that interact through respective penta-hedral (yellow dashed lines) and hexa-hedral (green dashed lines) coordination patterns with residues adjoining the selectivity filter residues S78, G233, G353 and G457. The ionic distances of 2.3-2.8 Å for Na^+ between V76, S77, S78, N231, C232 and H351, and of 2.6-2.9 Å for K^+ between V76, N231, C232, H351, N455 and V456, are formed between carbonyl oxygens of these residues (in sticks in atomic colours), located near selectivity filter residues. The K^+ ion effectively blocks the permeation channel through the protein pore, contrary to Na^+.

Figure 1

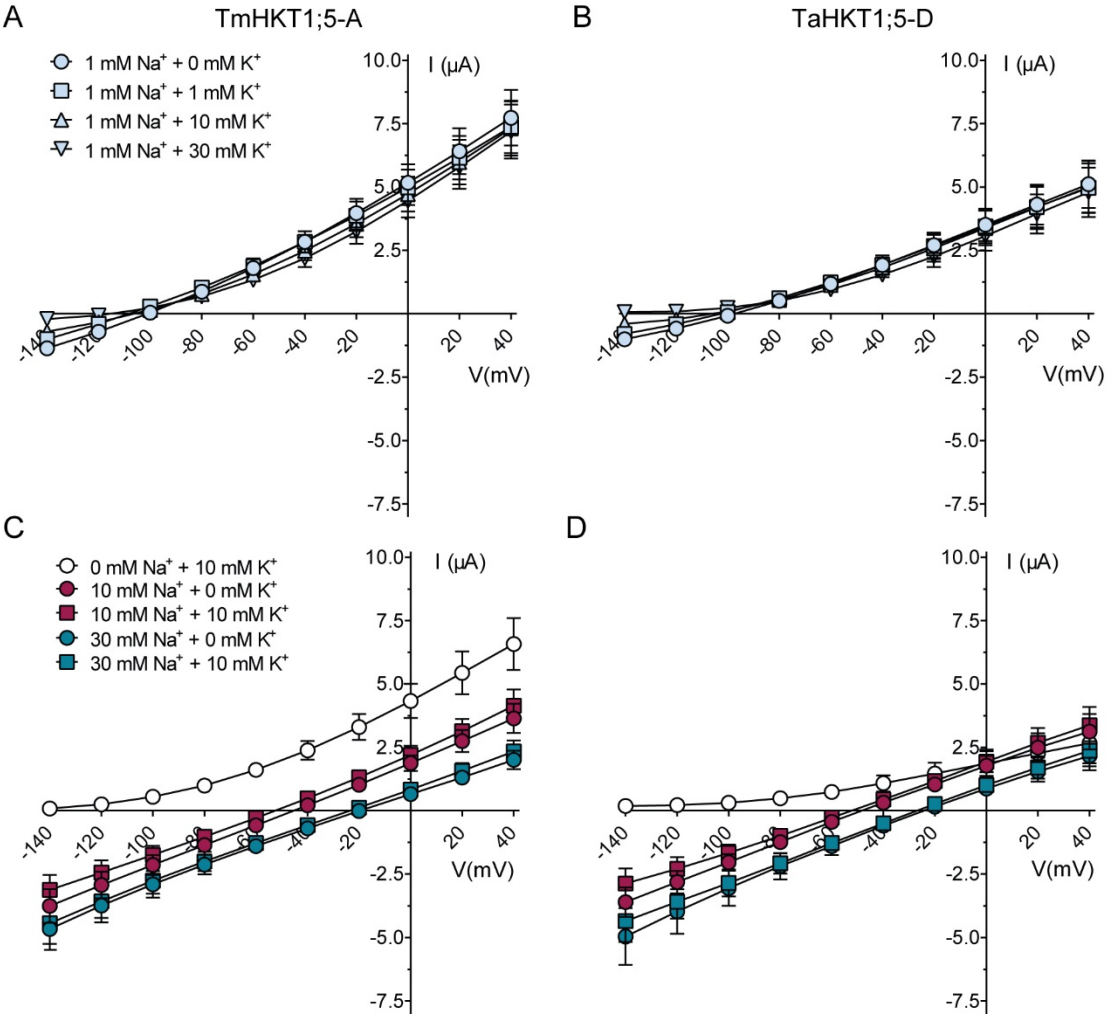

505 **Figure 2**

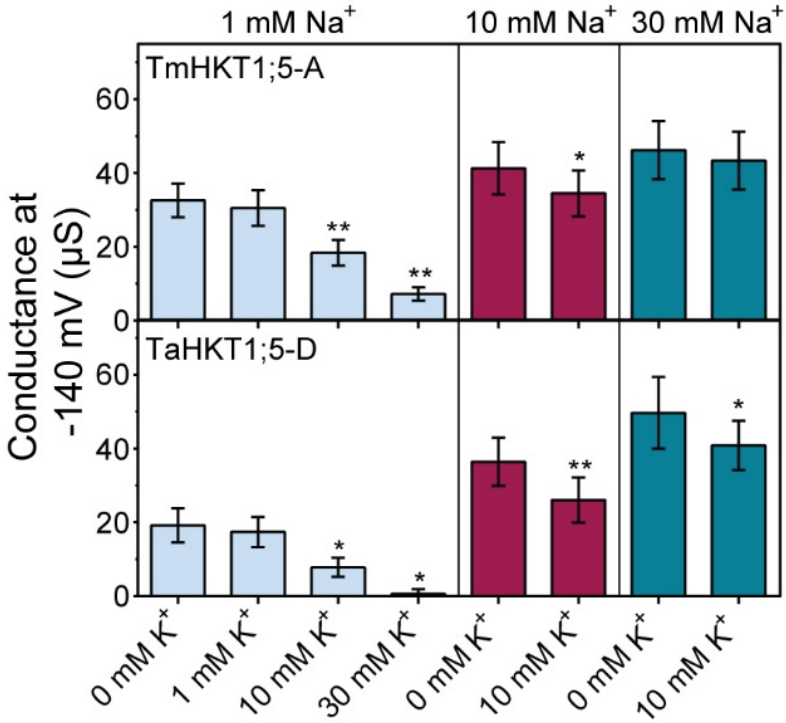

506

507

508 **Figure 3**

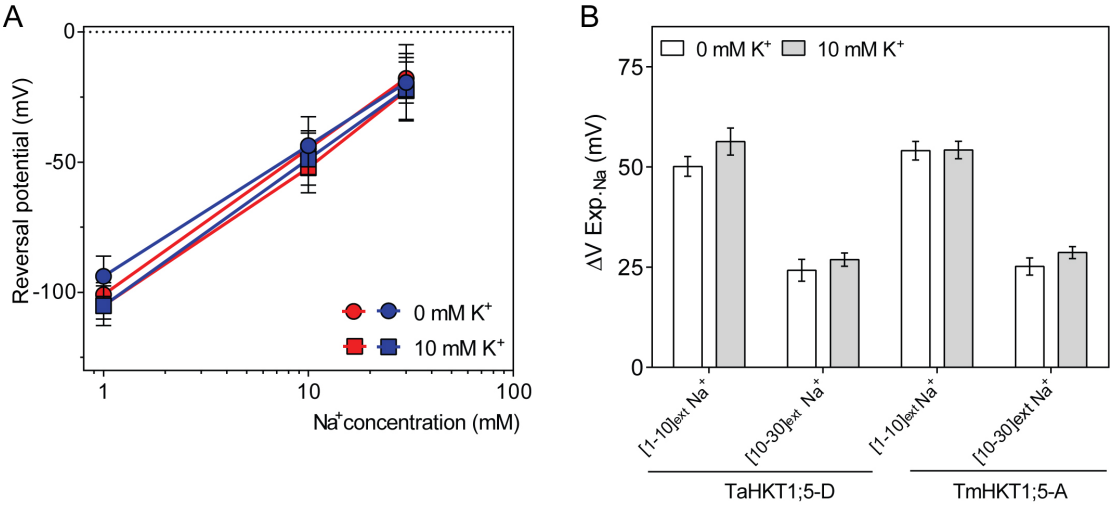

509

510

511 **Figure 4**

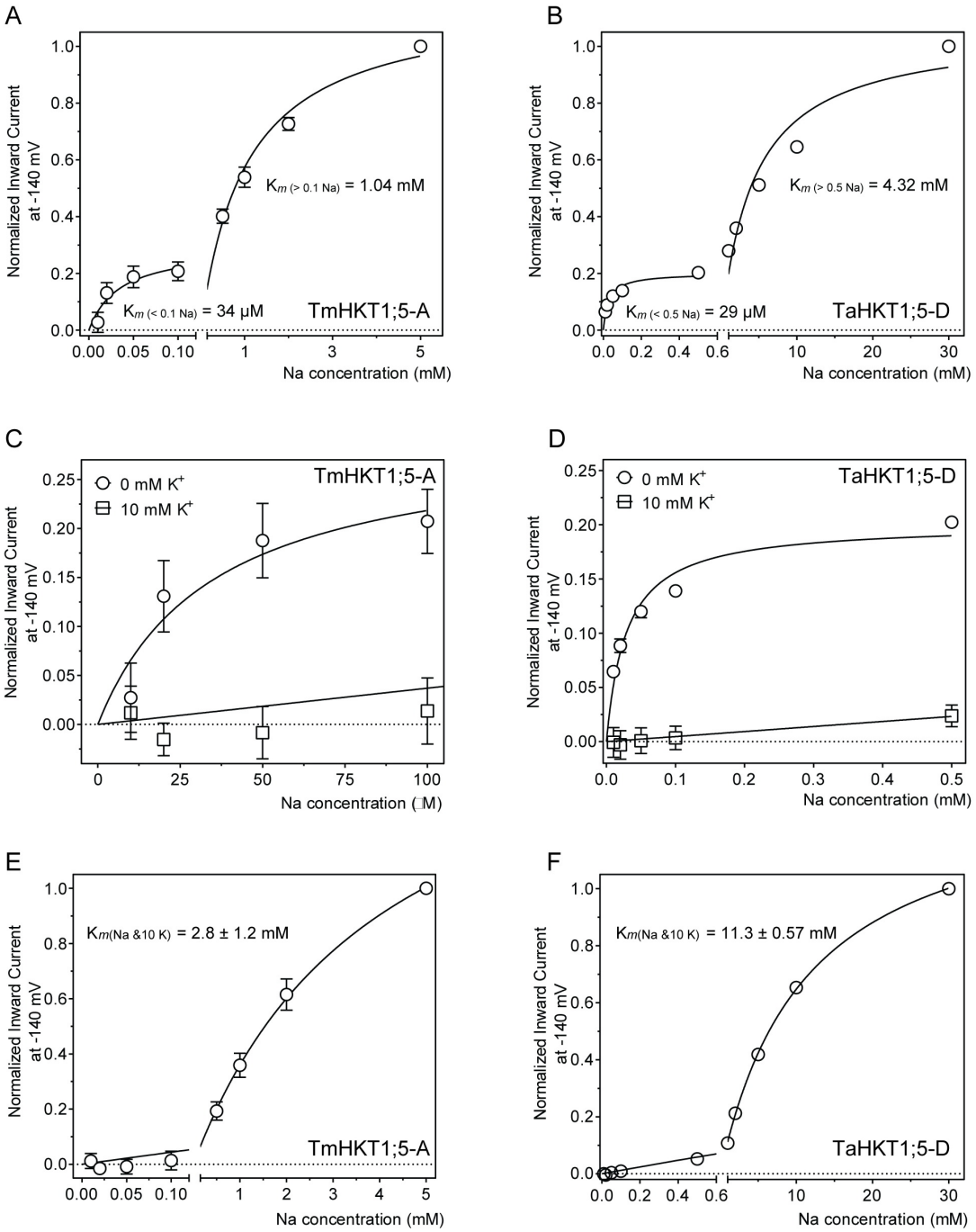

512

513

514

515 **Figure 5**

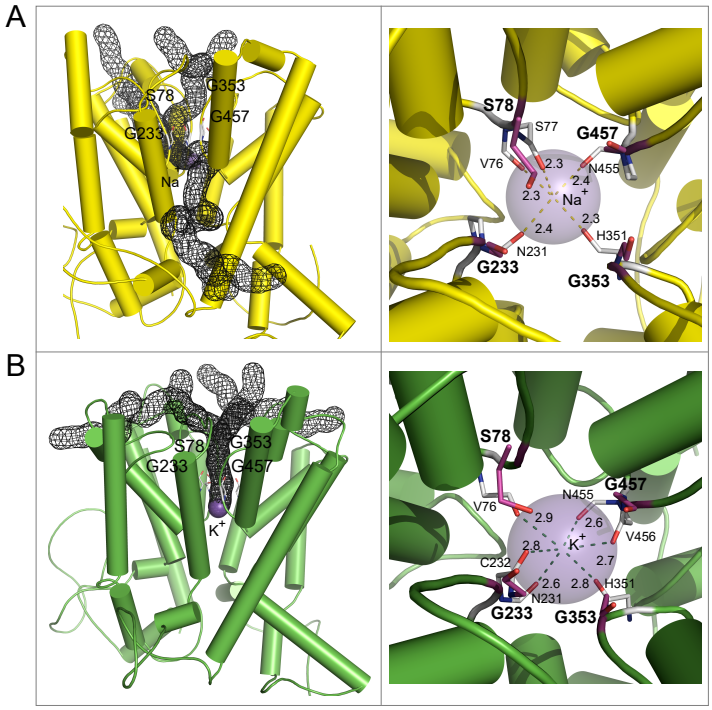

516
517